NEUROPHYSIOLOGY

Thalamic projections to the subthalamic nucleus contribute to movement initiation and rescue of parkinsonian symptoms

Glenn D. R. Watson[1]*, Ryan N. Hughes[1]*, Elijah A. Petter[1], Isabella P. Fallon[2], Namsoo Kim[1], Francesco Paolo Ulloa Severino[1,3], Henry H. Yin[1,2†]

The parafascicular nucleus (Pf) of the thalamus provides major projections to the basal ganglia, a set of subcortical nuclei involved in action initiation. Here, we show that Pf projections to the subthalamic nucleus (STN), but not to the striatum, are responsible for movement initiation. Because the STN is a major target of deep brain stimulation treatments for Parkinson's disease, we tested the effect of selective stimulation of Pf-STN projections in a mouse model of PD. Bilateral dopamine depletion with 6-OHDA created complete akinesia in mice, but Pf-STN stimulation immediately and markedly restored a variety of natural behaviors. Our results therefore revealed a functionally novel neural pathway for the initiation of movements that can be recruited to rescue movement deficits after dopamine depletion. They not only shed light on the clinical efficacy of conventional STN DBS but also suggest more selective and improved stimulation strategies for the treatment of parkinsonian symptoms.

INTRODUCTION

The rodent parafascicular nucleus (Pf) of the thalamus receives inputs from the cerebral cortex and provides a major projection to the basal ganglia (BG), a group of subcortical nuclei critical for action selection and movement initiation (*1*–*3*). Recent studies have focused on the function of Pf thalamostriatal projections, showing that the Pf significantly modulates striatal output and influences arousal, learning, and behavioral flexibility (*4*–*6*).

The Pf's connections with the BG have made it an exploratory target for deep brain stimulation (DBS) in patients with Parkinson's disease (PD), who show debilitating motor symptoms due to dopamine depletion. Pf DBS has been shown to improve the clinical symptoms of parkinsonian tremor and freezing of gait (*3*, *7*–*11*). It has been suggested that the efficacy of Pf DBS is due to the prominent Pf-striatum projections (*12*). However, the Pf is connected with other nuclei besides the striatum, including the globus pallidus and subthalamic nucleus (STN) (*13*, *14*). Much less is known about the functional importance of these connections. Of particular interest in this respect are Pf projections to the STN, a key nucleus that is heavily connected with the main BG nuclei and the most common target for DBS treatment for PD. Pf-STN projections and Pf-striatum projections originate in distinct neuronal populations (*13*, *15*). Because conventional DBS uses electrical stimulation, which nonselectively activates all afferent fibers, cell types, and fibers of passage, it is possible that Pf-STN projections could contribute to the therapeutic efficacy of conventional STN DBS.

In this study, using intersectional strategies to target specific neural pathways in mice, we investigated the functional contributions of the Pf and its projections to the striatum and STN. We found that the Pf-STN pathway, rather than the Pf-striatum pathway, mediates the generation of ipsiversive movements. Furthermore, selective optogenetic excitation of the Pf-STN pathway in bilateral 6-hydroxydopamine (6-OHDA) PD mice with complete akinesia restores locomotion and multiple natural behaviors. Finally, transsynaptic tracing of Pf-defined cells in the STN reveals a circuit comprising BG and brainstem nuclei that could mediate the observed rescue of PD symptoms using Pf-STN stimulation.

RESULTS

Pf neurons project to both the STN and striatum

Two major targets of the Pf are the striatum and STN. To visualize these projections, we injected canine adenovirus type 2 with Cre recombinase (CAV2-Cre) into the Pf of *Ai14* reporter mice (Fig. 1, A and B). Previous research has indicated that these projections originate from separate populations (*13*, *15*). However, Pf neurons projecting to the STN are located in the same region where projections to the dorsomedial striatum (DMS) originate (*16*). To further validate whether these are also separate neuronal populations, we injected a retrograde virus in both the DMS (pAAV-hSyn-DIO-eGFP) and STN (pAAV-hSyn-DIO-tdTomato) of *Vglut2-ires-Cre* transgenic mice ($n = 3$; Fig. 1, C and D). *Vglut2* is a selective marker for glutamatergic projection neurons in the thalamus, unlike cortical projection neurons that use *Vglut1* (*17*, *18*). Most of the Pf neurons projecting to the STN are separate from those projecting to the DMS (Fig. 1, D to F). However, given limited labeling of our retro-AAV experiment, it is possible that we may have underestimated the percentage of colocalized Pf neurons that project to both STN and DMS. However, in agreement with previous anatomical work in rats (*13*, *15*), our results suggest that Pf-STN and Pf-striatum pathways are largely segregated.

Unilateral optogenetic excitation of Pf Vglut2$^+$ neurons initiates movement

To understand the contribution of the Pf in movement generation, we optogenetically modulated Pf neural activity while monitoring movement kinematics during three-dimensional (3D) motion capture

[1]Department of Psychology and Neuroscience, Duke University, Durham, NC 27708, USA. [2]Department of Neurobiology, Duke University School of Medicine, Durham, NC 27708, USA. [3]Department of Cell Biology, Duke University School of Medicine, Durham, NC 27708, USA.
*These authors contributed equally to this work.
†Corresponding author. Email: hy43@duke.edu

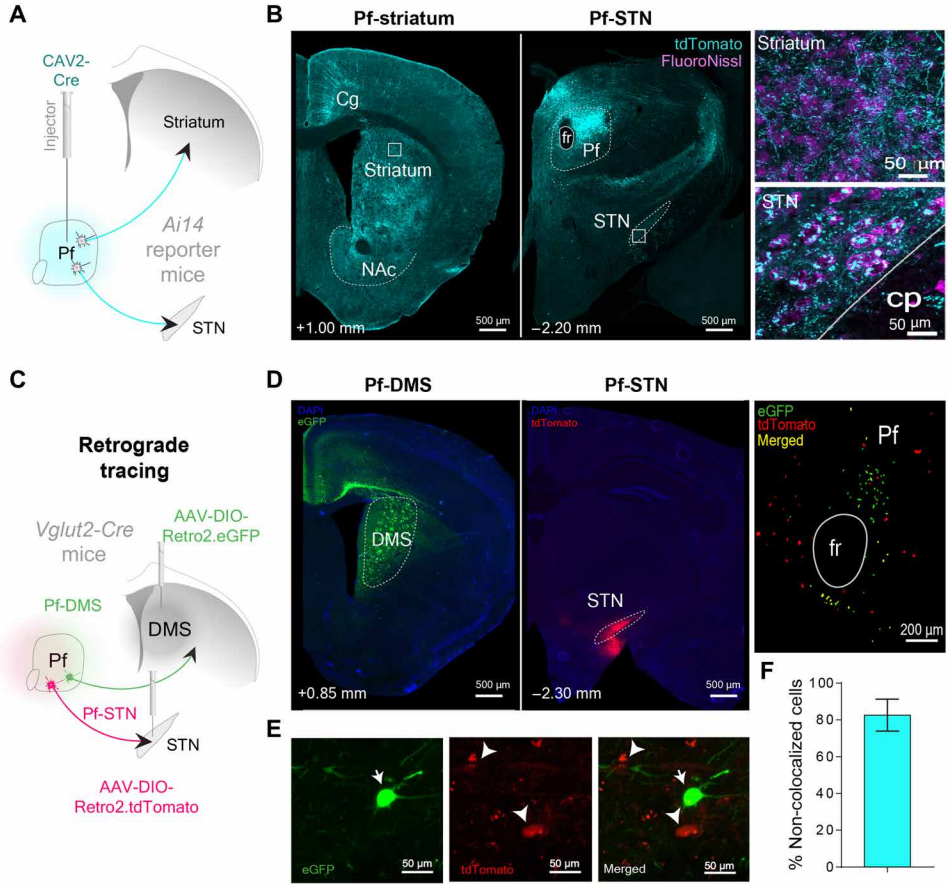

Fig. 1. Separate populations of Pf neurons project to the striatum and STN. (**A**) CAV2-Cre was injected into the Pf of *Ai14* transgenic mice to visualize afferent and efferent projections. Injection of high-titer CAV2-Cre allows visualization of both input and output connectivity by uptake both in the retrograde and anterograde directions. Neurons in *Ai14* mice fluoresce (tdTomato, cyan) when infected with a virus with Cre recombinase. (**B**) Pf terminal labeling in the striatum and STN. Insets show high-magnification view of Pf terminal labeling. (**C**) Cre-dependent retrograde viruses were injected into both the DMS and STN of Vglut2 mice ($n = 3$) to determine whether they are separate populations. (**D**) Pf terminals in either the DMS (left) or STN (middle) originate in topographically distinct Pf neurons (right). (**E**) Magnified view (100×) showing Pf-DMS and Pf-STN neurons. (**F**) Pf-DMS and Pf-STN neurons are mostly separate neuronal populations, as indicated by the total amount of Pf-DMS and Pf-STN neurons that do not colocalize with each other (82.63 ± 8.65%; mean ± SEM). Cg, cingulate cortex; cp, cerebral peduncle; fr, fasciculus retroflexus; NAc, nucleus accumbens; DAPI, 4′,6-diamidino-2-phenylindole; eGFP, enhanced green fluorescent protein.

of freely behaving mice in an open-field arena (Fig. 2A). To limit the excitation to Pf *Vglut2*$^+$ projection neurons, we injected an adeno-associated virus (AAV) with Cre-dependent channelrhodopsin (ChR2) in *Vglut2-ires-Cre* transgenic mice (Vglut2::ChR2^{Pf}, $n = 6$; Fig. 2A and fig. S8). We found that cell type–selective excitation of Pf *Vglut2*$^+$ neurons produced ipsiversive turning (Fig. 2B and movie S1). We found that increasing the stimulation frequency linearly increased the speed of ipsiversive turning, with each light pulse producing a relatively constant amount of turning (Fig. 2B). We furthermore confirmed that Pf neurons linearly increase their firing rate with increasing stimulation frequency using in vitro whole-cell patch clamp recording (fig. S1). We then tested whether optogenetic inhibition using the potent inhibitory channelrhodopsin (soma-targeted *Guillardia theta* anion-conducting ChR2, AAV1-SIO-stGtACR2) would produce the opposite effect by achieving potent optogenetic silencing of Pf *Vglut2*$^+$ neural activity (Vglut2::stGtACR2^{Pf}, $n =$ 8 hemispheres). Optogenetic inhibition can produce the opposite effect as excitation, producing contraversive rather than ipsiversive turning (fig. S1).

Unilateral optogenetic excitation of Pf projections to the STN produces movement

To elucidate the functional contributions of these distinct pathways from the Pf, we selectively excited the Pf-striatum or Pf-STN pathway. We injected a Cre-dependent virus containing ChR2 into the Pf of *Vglut2-Cre* mice and implanted optic fibers above the dorsal striatum (Vglut2::ChR2$^{Pf\text{-}striatum}$, $n = 8$; Fig. 2C). Unilateral terminal excitation of Pf-striatum neurons did not generate movement (Fig. 2D). Furthermore, no rotational movements were observed. However, considering the large rostrocaudal and mediolateral (ML) extent of the striatum, this strategy could be insufficient and only exciting a small fraction of Pf-striatum neurons. We therefore tested whether direct excitation of cell bodies in the Pf projecting to the striatum would generate movement. To achieve this, we injected AAV-Retro2-Cre, a virus with retrograde access to projection neurons into the striatum and a Cre-dependent virus containing ChR2 into the Pf of wild-type mice (Retro::ChR2$^{Pf\text{-}striatum}$, $n = 8$; Retro::eYFP$^{Pf\text{-}striatum}$ control, $n = 6$; Fig. 2C) (*19*). This retrograde strategy allows pathway-specific excitation of the cell bodies of neurons projecting throughout

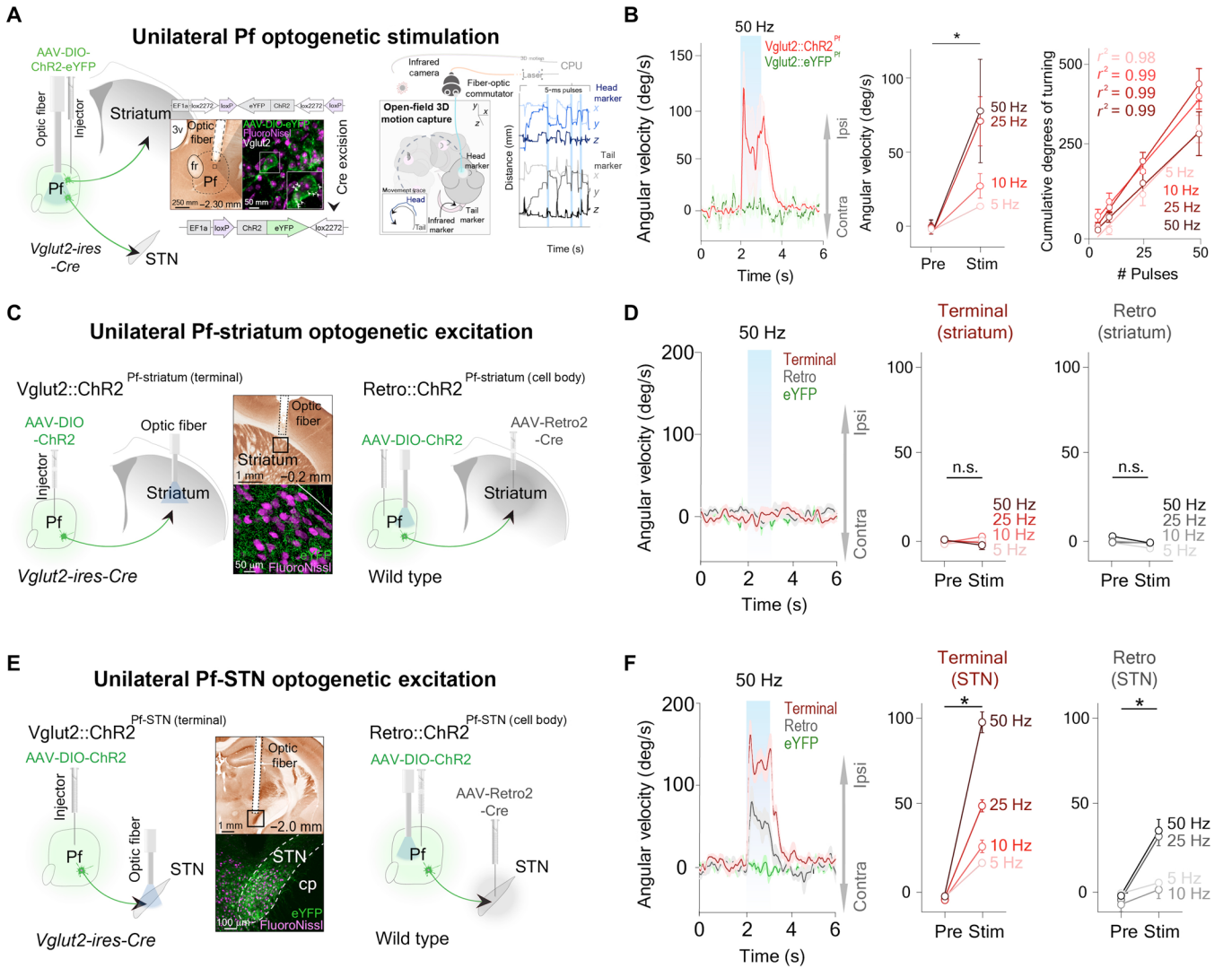

Fig. 2. Unilateral excitation of Pf and Pf-STN *Vglut2*$^+$ neurons initiates movement and causes ipsiversive turning, but Pf-STR does not. (**A**) Optic fiber placement above virally infected Pf *Vglut2*$^+$ neurons (left). Motion capture during optogenetic stimulation (right). (**B**) Unilateral excitation ($n = 6$) (left) increased ipsiversive angular velocity [$n = 6$, two-way repeated measures analysis of variance (RM ANOVA), before versus after stimulation ($F_{1,5} = 12.46$, $P = 0.017$, $n = 6$)]. Cumulative ipsiversive rotations in degrees (right) increased as a function of the number of ChR2 excitation pulses (all $r^2 \geq 0.98$). (**C**) Illustration of thalamostriatal (Pf-striatum) optogenetic experimental strategies during 3D motion capture. (**D**) No significant changes in angular velocity were observed during Pf-striatum cell body or terminal ChR2 excitation (two-way RM ANOVA, $P > 0.05$, $n = 8$; control mice, $n = 6$). (**E**) Schematic showing Pf-STN pathway–specific terminal stimulation and cell body stimulation. (**F**) Excitation of Pf-STN cell bodies and terminals caused a significant increase in ipsiversive angular velocity (two-way RM ANOVA, Pf-STN cell body: $F_{1,6} = 26.76$, $P = 0.0021$, $n = 7$; Pf-STN terminal: $F_{1,7} = 62.24$, $P < 0.0001$, $n = 8$; control mice, $n = 6$). Error bars indicate SEMs. n.s., not significant. eYFP, enhanced yellow fluorescent protein.

the striatum, thereby activating a much larger proportion of Pf-striatum neurons. We found that Pf-striatum cell body excitation also failed to generate movement (Fig. 2D).

We next tested whether excitation of Pf projections to the STN would generate the behavioral effects that we observed during nonspecific Pf activation (Fig. 2E). In contrast to our Pf-striatum results, we found that exciting terminals of Pf neurons projecting to the STN produces ipsiversive turning (Vglut2::ChR2$^{\text{Pf-STN}}$, $n = 8$; Fig. 2F, fig. S1, and movie S2). The kinematic effects from excitation produced ipsiversive turning, although it produced larger-radius turning than from the turning observed during nonspecific Pf *Vglut2*$^+$ excitation (fig. S2). We also replicated these results by exciting cell bodies of Pf neurons that project to the STN using the retrograde viral strategy previously described (Retro::ChR2$^{\text{Pf-STN}}$, $n = 8$; Retro::eYFP$^{\text{Pf-STN}}$ control mice, $n = 6$; Fig. 2, E and F). Together, these data demonstrate a nonstriatal route by which the thalamus can rapidly influence BG motor output, as well as provide evidence that the orienting and turning effects from excitation of Pf neurons are not mediated through thalamostriatal projections.

Bilateral optogenetic excitation of the Pf inhibits movement, whereas bilateral optogenetic excitation of Pf projections to the STN produces movement

Unilateral optogenetic stimulation of the Pf and the Pf-STN pathway both produced ipsiversive turning and orienting movements, although Pf-STN stimulation produced turning with a larger radius

(fig. S2). Pf-striatum stimulation, on the other hand, did not produce any effect. We then compared the effects of bilateral excitation of the Pf, Pf-striatum, and the Pf-STN pathway in an open-field arena by measuring the average distance traveled from a single session across all mice in each group (Vglut2::ChR2^{Pf}, n = 6, Vglut2::ChR2$^{Pf\text{-}striatum}$, n = 8, Vglut2::ChR2$^{Pf\text{-}STN}$, n = 8; Fig 3, A and B). Unexpectedly, nonspecific excitation of the Pf significantly slowed movement during stimulation epochs, as well as caused an increase in movement during nonstimulation epochs (Fig. 3, C and D). No significant changes in movement were observed with bilateral excitation in Pf-striatum animals (Fig. 3, E and F). In contrast, we found that Pf-STN terminal excitation significantly increased locomotion (Fig. 3, G and H). Thus, selective excitation of the Pf-STN pathway generates locomotion and plays a role in the initiation of movement. Furthermore, the distinct slowed movement seen in nonspecific Pf activation indicates that the Pf could be modulating movement generation in opposing ways through different output projections.

In sum, our optogenetic results reveal distinct behavioral effects depending on whether the Pf is globally activated or whether specific pathways are targeted. Bilateral nonspecific stimulation of the Pf slows movement, while bilateral stimulation of the Pf-striatum pathway has no effect. In contrast, bilateral stimulation of the PF-STN pathway initiates movement and produces locomotion (fig. S2).

Optogenetic excitation of Pf projections to the STN rescues motor deficits in a bilateral 6-OHDA parkinsonian mouse model

The STN is the most common target of traditional DBS treatment for PD. However, because traditional DBS uses electrical stimulation at extremely high frequencies, the underlying mechanisms remain controversial. It is unclear whether STN cell bodies, afferents from other structures, or fibers of passage are responsible for the therapeutic effects, nor is it clear whether neurons are excited or suppressed by DBS, as the high frequency stimulation could produce depolarization block. Our results suggest that some of the therapeutic benefits of traditional DBS of the STN could be attributed to excitation of Pf projections to the STN. To test this hypothesis, we used a bilateral 6-OHDA PD mouse model with bilateral dopamine depletion (Fig. 4A) (*20*, *21*). Because this bilateral PD model produces severe akinesia, it has been rarely used in previous research. Compared to the more commonly used unilateral 6-OHDA model, however, the bilateral 6-OHDA PD model more closely resembles severe PD, which is not typically restricted to one hemisphere. Moreover, the bilateral model provides the most stringent test for any rescue strategies.

To confirm dopamine depletion using the bilateral PD model, we quantified the resulting loss of tyrosine hydroxylase–positive neurons in the striatum immediately after experimental testing.

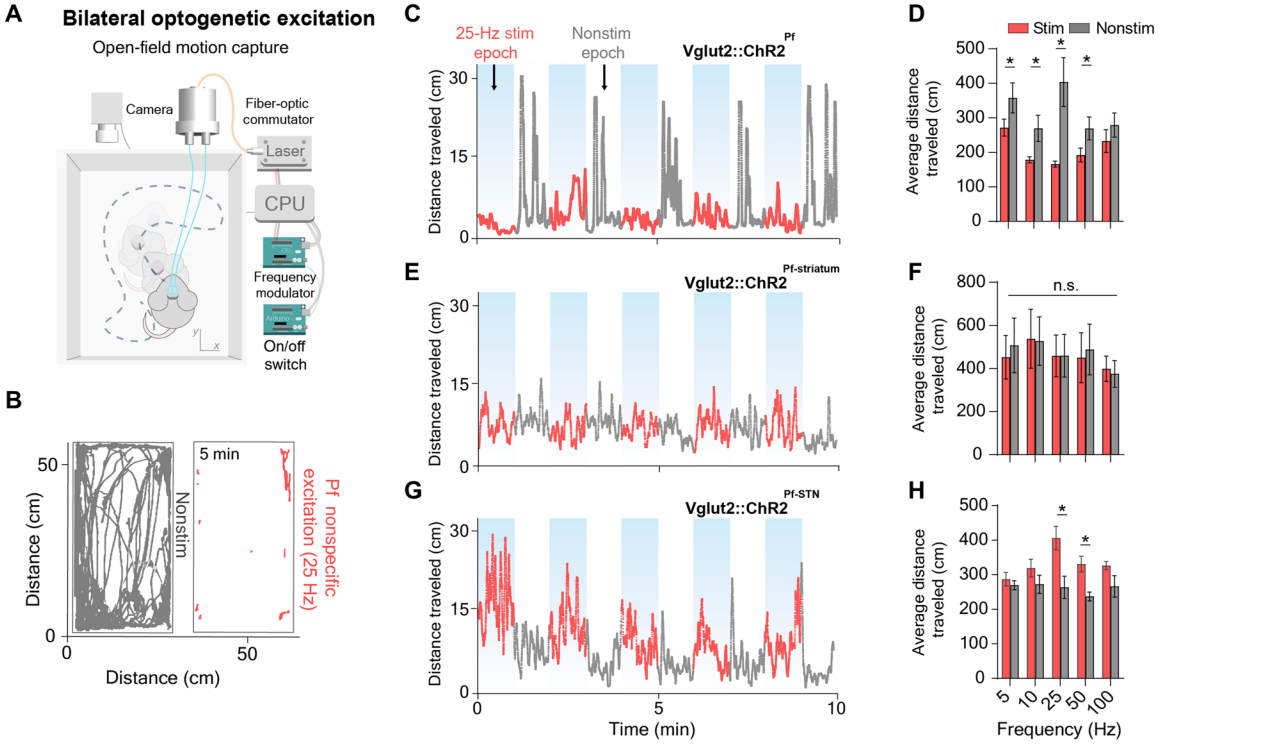

Fig. 3. Bilateral Pf-STN but not Pf-striatum pathway excitation increases locomotion, and nonspecific Pf stimulation reduces it. (**A**) For bilateral stimulation experiments, mice were placed in an open-field arena equipped with a motion capture camera. (**B**) Representative example of cumulative movement traces in the open field of stimulation and nonstimulation epochs. (**C**) Representative example of 25-Hz stimulation across the entire session for nonspecific Pf group (n = 6). (**D**) Nonspecific Pf excitation significantly reduced the average distance traveled compared to the nonstimulation epochs (two-way RM ANOVA, $F_{1,50}$ = 22.52, P < 0.0001). Post hoc comparison using Sidak's multiple comparison test indicated that 25 Hz was the only epoch that was significantly lower. (**E**) Representative example of 25-Hz stimulation across the entire session for Pf-striatum group (n = 8). (**F**) Pf-striatum excitation had no effect on distance traveled (P > 0.05). (**G**) Representative example of 25-Hz stimulation across the entire session for Pf-STN group (n = 8). (**H**) Pf-STN terminal excitation increased the average distance traveled compared to nonstimulation epochs (two-way RM ANOVA, ($F_{1,50}$ = 22.28, P < 0.0001, n = 5 mice). Post hoc tests indicated that the average distance traveled during 25 and 50 Hz epochs was significantly higher (P < 0.05).

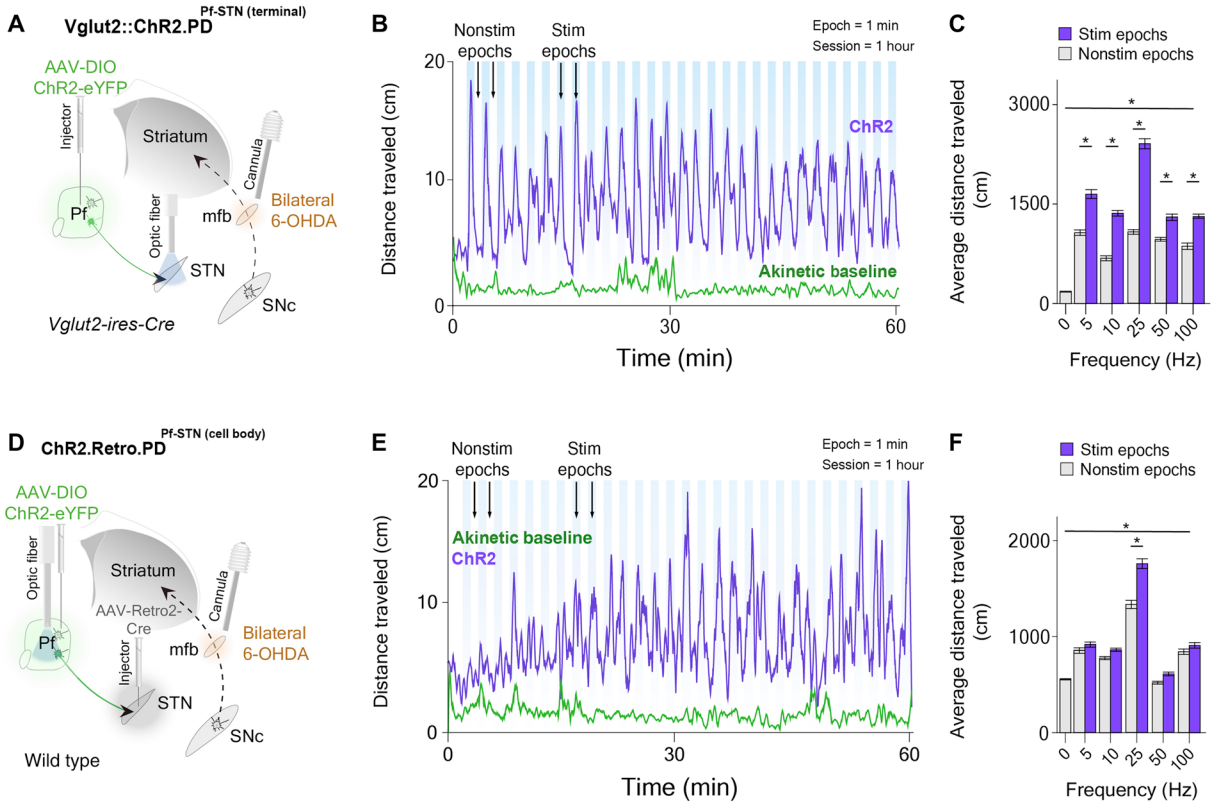

Fig. 4. Bilateral optogenetic Pf-STN terminal and cell body excitation in bilateral 6-OHDA parkinsonian mice rescue akinesia and promote locomotion. (**A**) An injection of AAV-DIO-ChR2 into the Pf of *Vglut2* mice allowed optogenetic excitation of Pf-STN terminals via an optic fiber implanted above the STN. Bilateral 6-OHDA injections into the mfb through guide cannulae generated a bilateral PD mouse model 4 weeks after viral injection. (**B**) Representative example of 25-Hz excitation of Pf-STN terminals showing increased distance traveled. (**C**) Pf-STN terminal excitation in bilateral PD mice increased the average distance traveled compared to the akinetic baseline condition (two-way RM ANOVA, $F_{2,60} = 0.7603$, $P < 0.0001$, $n = 5$). Post hoc comparisons using Tukey's multiple comparison test indicated that the average distance traveled during all stimulation epochs was significantly higher. (**D**) An injection of Retro-Cre into the STN paired with an injection of DIO-ChR2 into the Pf of wild-type mice allowed optogenetic excitation of Pf-STN cell bodies. (**E**) Representative example of 25-Hz optogenetic stimulation session of Pf-STN cell bodies showing increased distance traveled. (**F**) Pf-STN cell body excitation in bilateral PD mice significantly increased the average distance traveled compared to the akinetic baseline condition (two-way RM ANOVA, $F_{2,60} = 86.70$, $P < 0.0001$, $n = 5$).

Bilateral 6-OHDA injections caused >80% dopamine depletion in the striatum and nearly complete akinesia (fig. S3). Several days (3 to 7) after injecting the 6-OHDA, we optogenetically excited ChR2-infected Pf-STN terminals in *Vglut2*$^+$ mice while recording their movement in an open-field arena (Vglut2.PD::ChR2$^{\text{Pf-STN(terminal)}}$, $n = 5$; Fig. 4A and movie S3).

We found that Pf-STN terminal excitation in bilateral PD mice significantly increased locomotion compared to the akinetic baseline condition across all excitation frequencies (Fig. 4, B and C). These results indicate that Pf *Vglut2*$^+$ projections to the STN can be excited to rescue akinesia in bilateral PD mice.

We next examined whether optogenetic excitation of Pf-STN cell bodies would produce the same locomotor rescue in bilateral PD mice. To achieve this, we used the retrograde viral strategy in wild-type mice as previously described (Retro.PD::ChR2$^{\text{Pf-STN(cell-body)}}$, $n = 5$; Fig. 4D and movie S4). Unlike Pf-STN terminal excitation, we found a significant increase in locomotion compared to the akinetic baseline condition only during 25-Hz excitation (Fig. 4, E and F). These results indicate that exciting Pf terminals in the STN produces a more robust rescue of locomotion than exciting Pf-STN cell bodies.

To examine any long-term effect of repeated stimulations, we compared the average distance traveled among epochs during the first and last half of the experimental session (fig. S4). The mice traveled significantly greater distances in the first half of the session for the 5- and 10-Hz conditions during Pf-STN cell body excitation and in the 5-Hz condition during Pf-STN terminal excitation (fig. S4). However, there was no significant increase in all other conditions, most significantly in the 25-Hz condition where the most robust rescue effect was observed. These data indicate that stimulation of the Pf-STN pathway at higher frequencies can sustain the behavioral rescue effect.

Optogenetic excitation of Pf projections to the STN restores natural behaviors in a bilateral 6-OHDA parkinsonian mouse model

Spontaneous behaviors can be highly diverse. While traditional measures only focus on specific aspects of behavior (e.g., average distance traveled or velocity), they do not provide a comprehensive view of different types of behaviors affected by a neural manipulation. To quantify natural behavioral states during our PD rescue experiments, we applied an unsupervised autoregressive hidden Markov model

(AR-HMM) to our 2D video recordings (fig. S5) (*22*). This technique allows for more precise and unbiased classification of behavioral states than traditional measures (*22*, *23*).

Each video frame [50 frames per second (f/s)] was assigned a behavioral label or "state," which was used to calculate the probability of using each behavioral state, as well as the probabilities of transitioning between these states (fig. S5). We further clustered the AR-HMM identified behaviors into kinetic and akinetic groups that revealed a rescue of distinct kinetic behavioral states during both Pf-STN terminal and cell body optogenetic excitation in bilateral PD mice (Fig. 5 and figs. S6 and S7).

If we compare the baseline akinetic condition to the stimulation epochs, then excitation restored multiple natural behaviors, including locomotion, turning, perimeter exploration, rearing, and head movement. The probability of being in the kinetic behavioral states during excitation approached that of control animals in numerous behaviors, most prominently in the Pf-STN terminal group (Fig. 5A and fig. S6). More robust rescue effects are observed in the Pf-STN terminal excitation group than in the Pf-STN cell body group, including locomotion, turning, and perimeter exploration. It also significantly reduced immobility behaviors (Fig. 5B and fig. S6). This behavioral rescue is shown by the higher probability of kinetic behaviors and lower probability of akinetic behaviors during optogenetic excitation.

To measure action initiation and switching, we quantified their probability of transitioning between kinetic behavioral states during optogenetic excitation. We found that excitation of the Pf-STN pathway increased the probability of transitioning between kinetic behavioral states. In the akinetic condition, the opposite is found, where a higher probability of transitioning between akinetic behavioral states is observed (Fig. 5C and fig. S6). The most robust increase in transition probabilities between kinetic states was observed in the

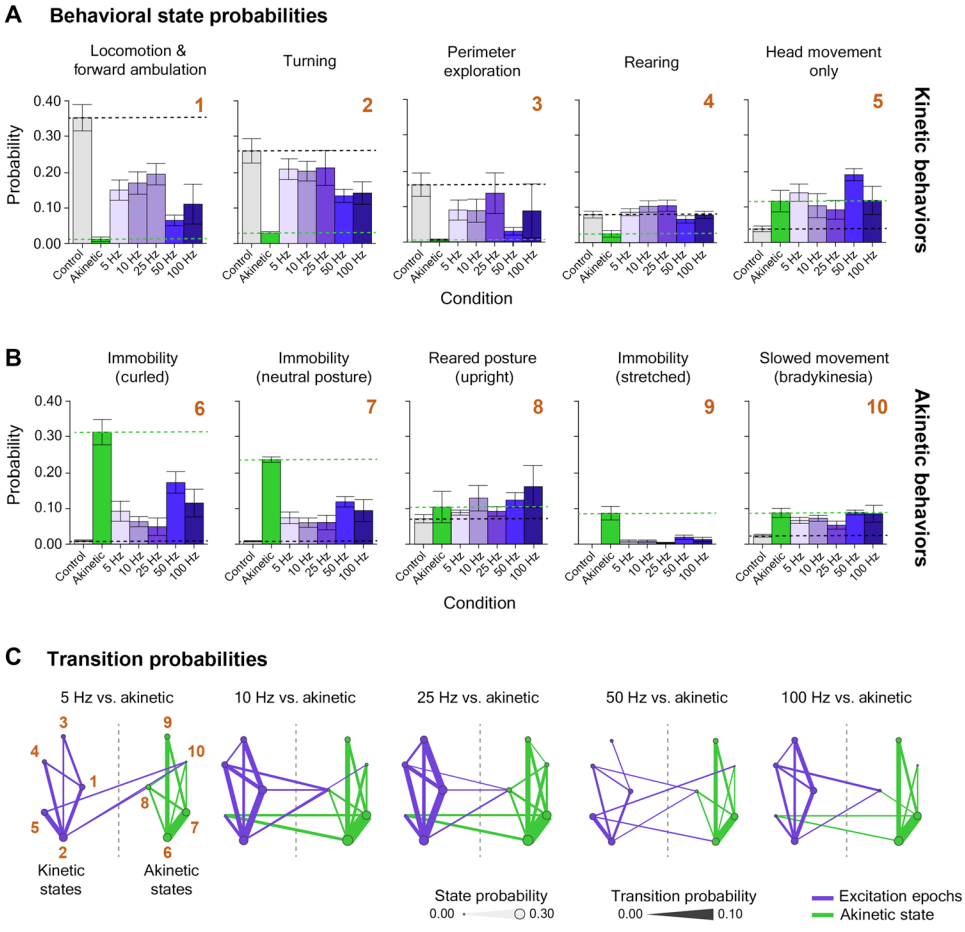

Fig. 5. Optogenetic excitation of Pf-STN terminals in bilateral 6-OHDA parkinsonian mice restores natural behaviors. (**A**) A machine learning algorithm was used to parse behaviors before and after optogenetic stimulation. Probability of kinetic behavioral states during Pf-STN terminal excitation epochs (ChR2, purple) across all frequencies except 5 Hz in bilateral 6-OHDA PD mice. All kinetic behavioral states were significantly higher during stimulation compared to akinetic baseline and control [Hotelling's *t* tests, $P < 0.0001$ for all comparisons except 5 Hz ($P > 0.05$)]. (**B**) Akinetic behavioral states were significantly different during stimulation compared to akinetic baseline and control [Hotelling's *t* tests, $P < 0.0001$ for all comparisons except 5 Hz ($P > 0.05$)]. Numbers (gold) represent identified behavioral states used in (C). (**C**) Pf-STN terminal excitation increases transition between kinetic behavioral states compared to the akinetic baseline condition. Bigrams illustrate transition probabilities between kinetic (left) and akinetic (right) states. Circle diameter represents the same behavioral state probabilities shown in (B). Line thickness represents the transition probability. Numbers represent behavioral states identified in (B): (1) locomotion and forward ambulation, (2) turning, (3) perimeter exploration, (4) rearing, (5) head movement only, (6) immobility (curled), (7) immobility (neutral posture), (8) reared posture, (9) immobility (stretched), and (10) slowed movement (bradykinesia). Bigrams for analysis can be found in fig. S7. Error bars indicate SEMs.

25-Hz condition. Collectively, these data demonstrate that excitation of the Pf-STN pathway and, in particular, Pf-STN terminals reduces PD motor deficits and increases the occurrence of kinetic behaviors.

Pf-defined projections through the STN transsynaptically target output nuclei of the BG and brainstem locomotor regions

To reveal the potential circuitry responsible for our Pf-STN PD rescue, we first visualized inputs to the Pf using viral-based retrograde tracing by injecting CAV2-Cre into the Pf of *Ai14* reporter mice (Fig. 6A). Our CAV2-Cre retrograde tracing shows strong inputs from midbrain neuromodulatory and reticular activating areas, such as the laterodorsal tegmental nucleus, pedunculopontine nucleus (PPN), medial reticular formation, and locus coeruleus (Fig. 6, B to F). Numerous brain regions implicated in detection of salient stimuli also project to the Pf, including the superior colliculus, cuneiform nucleus, parabrachial nucleus, and cingulate cortex. Numerous Pf afferents were also seen from sensorimotor brain regions (primary motor and sensory cortices, zona incerta, and deep cerebellar nuclei) and nuclei of the BG [entopeduncular nucleus, external globus pallidus, and substantia nigra pars reticulata (SNr); Fig. 6, B to F].

We next elucidated downstream circuits that can be affected by activation of the Pf-STN pathway by uncovering the downstream targets of STN neurons that receive synaptic contacts from Pf neurons using viral-based transsynaptic tracing (*24*). To visualize these Pf-defined STN projections, we first injected a fluorescently tagged (tdTomato) Cre-expressing virus into the Pf of wild-type mice (Fig. 6G). This virus enables anterograde transsynaptic spread of Cre into postsynaptically targeted neurons. We then injected a fluorescently tagged [enhanced yellow fluorescent protein (eYFP)] Cre-dependent virus into the STN to visualize STN projections with Pf inputs. In other words, only STN neurons that are postsynaptic targets of the Pf will express eYFP. We found that Pf-defined STN efferents terminate in various BG output nuclei, including the SNr, the external globus pallidus, the entopeduncular nucleus (the rodent homolog of the internal globus pallidus), and other key brainstem regions for motor control (Fig. 6, H to K). This finding shows that, independent of the striatum, the Pf can influence BG output nuclei and brainstem locomotor regions through the STN (Fig. 6, L and M). These regions, in turn, also project to the Pf. Furthermore, these results are in agreement with previous observations that activation of BG output nuclei, such as the SNr, produces ipsiversive turning and mediates posture control (*25*, *26*).

DISCUSSION

We showed that the Pf can influence movement initiation primarily through its projections to the STN. Our findings suggest that the Pf-STN pathway could be part of a circuit for orienting and steering in mice. Given the strong afferents from neuromodulatory and sensorimotor brain regions, the Pf is anatomically positioned to combine somatosensory and proprioceptive information (Fig. 6). Moreover, we identified downstream locomotor brain regions that could mediate the movement effects observed during Pf-STN optogenetic excitation with viral-based transsynaptic tracing (Fig. 6).

An interesting finding was that bilateral Pf excitation resulted in slowed movement (Fig. 3 and fig. S2). This could be due to simultaneous activation of antagonistic units (e.g., leftward and rightward) from the two hemispheres. With the unilateral stimulation experiments, the turning produced by Pf-STN stimulation appeared to be distinct from turning produced by nonspecific Pf stimulation (compare movies S1 and S2). Unilateral stimulation of the Pf-STN pathway usually produced larger-radius turning with a larger forward component, whereas nonspecific stimulation usually produced tight circling with a backward component. This difference could be due to the recruitment of additional pathways from the Pf when stimulated nonselectively, including the Pf-striatum pathway. By contrast, bilateral Pf-STN excitation resulted in locomotion and movement initiation (Fig. 3 and fig. S2). Given the specificity in targeting a single pathway, this strongly suggests that the Pf-STN pathway plays an important role in generating locomotor rhythms and initiating large, fast orienting movements.

Our results thus suggest a functionally novel pathway regulating action initiation. Traditionally, action initiation is thought to be regulated by the direct and indirect pathways of the BG, via their effects on the BG output to the brainstem and thalamic targets. BG pathways are modulated by dopamine and undergo profound changes following chronic dopamine depletion as in PD (*12*, *27*). Stimulation of the striatum can produce contraversive turning (*28*, *29*) and alleviate PD motor symptoms (*30*). However, we showed that, unexpectedly, the Pf-STN pathway, rather than the Pf-striatum pathway, is critical for movement initiation. Because we injected a large total volume of virus throughout the anterior-posterior (AP) axis of the Pf, some regions besides the Pf could have been stimulated. However, activation of these other areas is unlikely to be responsible for our observations because the Pf is the only known intralaminar nucleus that projects to the STN and because we positioned our optic fibers at an angle so that other areas are unlikely to be stimulated. Moreover, it is also unlikely that our failure to elicit movements with Pf-striatum stimulation is due to the limited number of striatal neurons affected in our experiments. Unilateral striatal activation generates contraversive turning (*28*–*30*), whereas we showed that unilateral Pf or Pf-STN activation produced ipsiversive turning. Consequently, the observed behavioral effects cannot be attributed to the engagement of the basic BG circuitry via the striatum.

Another established pathway for action initiation is the "hyperdirect" pathway from the motor cortex to the STN (*31*). This pathway can bypass the striatum, the major input nucleus of the BG, and directly affect BG output. Here, we identified a "superdirect" pathway that can also bypass the BG input nuclei and directly affect BG output, as well as further downstream motor nuclei directly. Instead of relying on the motor cortical projections to the STN, this pathway originates in the Pf, which is part of the reticular activating system and plays an important role in arousal and orienting. For example, it receives a strong projection from midbrain nuclei such as the superior colliculus and can thus modulate orienting and locomotor signals that bypass the cortex and striatum (Fig. 6). Its direct efferent projections can also bypass the BG output nuclei and directly influence brainstem nuclei responsible for movement and locomotion, as shown by our transsynaptic tracing results (Fig. 6).

Potential clinical implications

The Pf-STN pathway thus provides a circuit mechanism that could explain the clinical efficacy of DBS for relief of PD motor symptoms. We demonstrated notable rescue of akinesia in bilateral PD mice using selective targeting of the Pf-STN pathway (Figs. 4 and 5 and fig. S6). In our bilateral 6-OHDA model, there is virtually complete akinesia, yet we were also able to markedly restore movement with

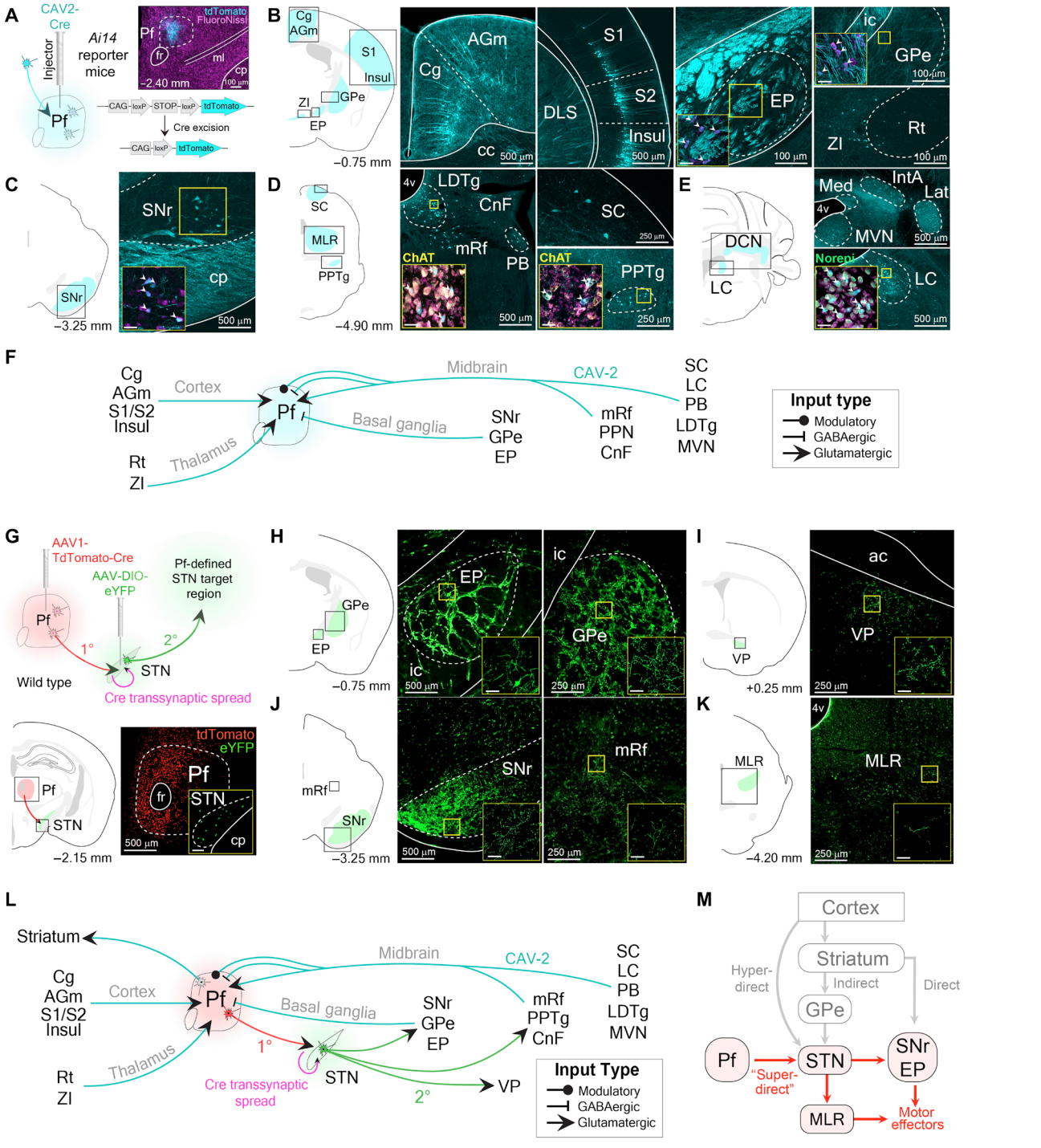

Fig. 6. Viral retrograde tracing reveals that the Pf connectivity with BG and brainstem locomotor regions. (**A**) Representative example of CAV2-Cre injection into the Pf of an *Ai14* transgenic mouse to visualize afferent projections. (**B** to **E**) Retrograde labeled cells from Pf CAV2-Cre injection shown in (A). Cells were found in agranular medial cortex (AGm), Cg, entopeduncular nucleus (EP; rodent homolog of primate internal segment of the globus pallidus), external segment of the globus pallidus (GPe), insular cortex (Insul), reticular nucleus (Rt), S1, S2, and zona incerta (ZI) (B); SNr (C); cuneiform nucleus (CnF), laterodorsal tegmental nucleus (LDTg), mesencephalic reticular formation (mRf), parabrachial nucleus (PB), PPN, and superior colliculus (SC) (D); interposed anterior nucleus of the cerebellum (IntA), lateral cerebellar nucleus (Lat), locus coeruleus (LC), medial cerebellar nucleus (Med), and medial vestibular nucleus (MVN) (E). Insets show retrograde labeled cells colocalized with neuromodulatory cell type markers [choline acetyltransferase (ChAT) and norepinephrine (Norepi)]. (**F**) Summary schematic of viral-based retrograde Pf anatomy results. (**G**) Top: Injection of tdTomato-Cre into Pf (first-order neuron) allows transsynaptic spread of Cre into the STN. AAV-DIO-eYFP was subsequently injected into the STN (second-order neuron) to visualize Pf-defined subthalamic projections. Bottom: Illustration and histological confirmation showing Pf and STN injections. (**H** to **K**) Coronal sections show terminal labeling sites of Pf-defined subthalamic targets. (**L**) Schematic of viral-based retrograde Pf and transsynaptic Pf-STN anatomy results. (**M**) Schematic of the superdirect pathway. ac, anterior commissure; cc, corpus callosum; DCN, deep cerebellar nuclei; ml, medial lemniscus; MLR, midbrain locomotor region.

selective Pf-STN stimulation. In particular, stimulation increased the transition probability of numerous natural behavioral states that are difficult to quantify with conventional measures. For instance, Pf-STN excitation in our bilateral PD mice alleviated numerous symptoms such as gait immobility and promoted natural locomotion and postural rearing (Fig. 5 and fig. S6). Note that, in human patients, such symptoms are not satisfactorily treated using conventional DBS approaches and are often resistant to medication (*3*, *32*–*34*). It is therefore possible that exciting Pf inputs to the STN in patients with PD could abolish pathological STN activity, thus reducing akinesia and promoting volitional movements (*35*, *36*).

Previous work has shown that optogenetic excitation of STN neurons did not rescue akinesia but that inputs from motor cortex were more important (*37*). Our results suggest that a subset of STN neurons receiving Pf inputs may be critical for rescuing akinesia. Thus, the therapeutic effects of STN-DBS could be due to the activation of Pf glutamatergic afferents to the STN, in addition to those from the motor cortex. This possibility is also supported by a recent study demonstrating increased locomotion in dopamine-depleted mice by optogenetically exciting parvalbumin-positive neurons in the external segment of the globus pallidus (GPe) (*21*). These GPe neurons also project to the Pf (*38*), suggesting a potential circuit that can be recruited to generate movement in PD mice.

Pf-STN terminal excitation in bilateral PD mice was more effective at alleviating akinesia than Pf-STN cell body excitation (compare Fig. 5 and fig. S6). Bilateral intralaminar DBS (targeting Pf and centromedial nucleus) in patients with PD has limited therapeutic benefits compared to STN-DBS (*7*, *9*, *39*). Given our finding that nonspecific bilateral optogenetic excitation resulted in slowed movement (Fig. 3 and fig. S2), intralaminar DBS in patients with PD may recruit conflicting downstream neural circuits that reduces its therapeutic efficacy. In contrast, in this study, bilateral Pf-STN excitation was shown to promote movement (Fig. 3 and fig. S2). This could explain why nonspecific intralaminar DBS has limited therapeutic value for most PD symptoms.

We found that low-frequency excitation (25 Hz) was more effective than high-frequency excitation at restoring movement in bilateral PD mice (Figs. 4 and 5 and fig. S6). This is unexpected because conventional STN-DBS for PD requires very high frequencies (100 to 130 Hz). However, conventional DBS uses electrical stimulation that nonselectively activates all afferent fibers, cell types, and fibers of passage. It is therefore possible that Pf neurons projecting to the STN could have different therapeutic stimulation parameters. Recent work showed that, in dopamine-depleted mice, only high-frequency optogenetic stimulation of the STN was effective at alleviating motor deficits (*40*). This finding suggests that stimulation of STN neurons has different effects than the activation of the Pf-STN pathway. It is possible that distinct populations of STN neurons have different functions and low-frequency stimulation is only effective when applied to STN neurons receiving Pf projections.

Using transsynaptic viral tracing of downstream structures, we identified that STN neurons receiving Pf afferents project to the PPN, a key component of the mesencephalic locomotor region. It has been shown that PPN-DBS in patients with PD improves levodopa/STN-DBS–resistant axial symptoms (e.g., freezing of gait and postural instability) during low-frequency DBS (~25 Hz), which are the symptoms rescued by our Pf-STN stimulation (*7*, *36*, *41*). Further investigations are necessary to elucidate the role of the Pf-STN projections to the PPN.

CONCLUSION

Collectively, our results suggest that Pf-STN projections provide the Pf with direct access to BG output nuclei and other brainstem regions critical for locomotion and other behaviors (*31*). This circuit could be critical for steering during locomotion and for rapid orienting toward salient stimuli, while Pf thalamostriatal projections can influence higher-order functions such as regulation of attention, action sequences, and switching. With the development of viable optogenetic tools for human use, as well as more precise surgical targeting of the Pf-STN axons, it may be possible to improve DBS treatments for PD symptoms by selectively activating this pathway.

MATERIALS AND METHODS

All experimental procedures were conducted in accordance with standard ethical guidelines and were approved by the Duke University Institutional Animal Care and Use Committee. All behavioral data were collected from wild-type (C57BL/6J; the Jackson laboratory) and *Vglut2-ires-Cre* mice (Slc17a6$^{tm2(cre)Lowl}$; the Jackson laboratory). *Vglut2-ires-Cre* mice have Cre recombinase expression under the control of *Vglut2* receptor regulatory elements without disrupting endogenous vesicular glutamate transporter 2 (Vglut2) expression. Optogenetic control of Pf glutamatergic neurons was achieved with a double-floxed inverted recombinant AAV5 virus injection to express the excitatory opsin ChR2-eYFP. Viral infection in the Pf was histologically verified with eYFP imaging colocalized against a Vglut2 antibody and 4′,6-diamidino-2-phenylindole (DAPI) staining. Wild-type mice were used for pathway-specific retrograde Cre expression and retrograde and transsynaptic tracing experiments. Retrograde anatomical tracing data were collected from Ai14 reporter mice [129S6-Gt(ROSA)26Sor$^{tm14(CAG-tdTomato)Hze}$/J; the Jackson laboratory]. Ai14 reporter mice harbor a loxP-flanked STOP cassette that is excised in the presence of Cre to promote transcription of a CAG promoter–driven red fluorescent protein variant (tdTomato). A high titer (~3.0×10^{13} genome copies per ml) was used to visualized input-output connectivity. For PD experiments, *Vglut2-ires-Cre* mice were used for Pf-STN terminal excitation experiments, and wild-type mice were used for Pf-STN cell body excitation experiments.

Viral constructs

CAV2-Cre was obtained from Institut de Génétique Moléculaire de Montpellier. rAAV5.EF1α.DIO.hChR2(H134R).eYFP, rAAV5.EF1α.DIO.eYFP, AAV1.hSyn.tdTomato.Cre, and AAV(Retro2).hSyn.EF1α.Cre.WPRE were obtained from the Duke University Vector Core. pAAV_hSyn1-SIO-stGtACR2-FusionRed was from O. Yizhar (Addgene viral prep no. 105677-AAV1; RRID:Addgene_105677). pAAV-hSyn-DIO-eGFP was a gift from B. Roth (Addgene viral prep no. 50457-AAVrg; http://n2t.net/addgene:50457; RRID:Addgene_50457).

Surgery

Mice were anesthetized with 2.0 to 3.0% isoflurane mixed with oxygen (0.60 liter/min) for surgical procedures and placed into a stereotactic frame (David Kopf Instruments, Tujunga, CA). Meloxicam (2 mg/kg) and bupivacaine (0.20 ml) were administered before incision. To interrogate Pf during open-field experimentation, adult *Vglut2-ires-Cre* mice were randomly assigned to Vglut2::ChR2^{Pf} ($n = 5$, 2 males and 3 females, 8 to 10 weeks old) or Vglut2::eYFP^{Pf} groups ($n = 4$, 2 males and 2 females, 8 to 10 weeks old). Craniotomies were made bilaterally above the Pf, and virus was microinjected through a pulled glass

pipette at various penetrations and depths (0.6 μl each hemisphere; AP: −2.10 to 2.50 mm relative to bregma, ML: ±0.60 to 0.75 mm relative to bregma, and dorsoventral (DV): −3.70 to 3.10 mm from skull surface) using a microinjector (Nanoject 3000, Drummond Scientific). For pathway-specific open-field experiments, wild-type mice were used to selectively target the cell bodies of Pf-striatum (n = 5, 3 males and 2 females, 8 to 10 weeks old) and Pf-STN (n = 6, 2 males and 4 females, 8 to 10 weeks old) neurons by bilaterally injecting AAV(retro2).hSyn.EF1α.Cre.WPRE into the entire rostrocaudal and ML extent of the striatum (1 μl each hemisphere; AP: +1.35 to −0.75 mm relative to bregma, ML: ±1 to 2.75 mm relative to bregma, and DV: 2.0 to 3.50 mm from skull surface) or the STN (AP: −1.90 to −2.20 mm relative to bregma, ML: ±1.40 to 1.80 mm relative to bregma, and DV: 4.10 to 4.40 mm from skull surface) in parallel with a Cre-dependent ChR2 virus injection into the Pf. For Pf cell body stimulation, custom-made optic fibers (length below ferrule, 5 to 6 mm; >80% transmittance; core diameter, 105 mm) were implanted directly above the nucleus (AP: −2.30 mm relative to bregma, ML: ±1.20 to 1.30 mm relative to bregma, and DV: 2.70 to 2.80 mm from skull surface, 10°). Pf-STN terminals (n = 5, 3 males and 2 female, 8 to 10 weeks old) were targeted with optic fibers implanted directly above the STN (AP: −1.80 to 2.0 relative to bregma, ML: ±1.50 to 1.60 mm relative to bregma, and DV: 4.20 mm from skull surface). Pf-striatum terminals (n = 5, 2 males and 3 female, 8 to 10 weeks old) were targeted with optic fibers implanted directly above the dorsal striatum (AP: 0.25 to −0.50 mm relative to bregma, ML: ±2.50 to 2.90 mm relative to bregma, and DV: 1.75 mm from skull surface). Pf-STN (n = 6, 3 males and 3 females, 10 to 12 weeks old) and Pf-striatum (n = 6, 2 males and 4 females, 10 to 12 weeks old) controls were generated using the retrograde access viral technique previously described paired with an injection of rAAV5.EF1α.DIO.eYFP into and fiber implants above the Pf. For retrograde anatomy experiments (n = 3, 2 males and 1 female, 8 to 10 weeks old), 15 to 20 nl of CAV2-Cre was injected into the Pf at one depth to prevent leakage (AP: −2.30 mm relative to bregma, ML: ±0.65 to 0.75 mm relative to bregma, and DV: 3.60 to 3.30 mm from skull surface). For transsynaptic tracing experiments (n = 3, 1 male and 2 females, 8 to 10 weeks old), AAV1.hSyn.tdTomato.Cre was injected into the Pf and rAAV5-EF1α-DIO-eYFP was injected into the STN using the coordinates previously listed. For all virus injections, the pipette sat at the last injection depth of each penetration for 20 min before being withdrawn from the brain to facilitate uptake. Bilateral PD mice (n = 13, 7 males and 6 females, 8 to 10 weeks old) were generated by implanting 15-gauge (length, 7 mm) guide cannulae implanted above the medial forebrain bundle (mfb) (AP: −0.95 mm relative to bregma, ML: ±3.10 mm relative to bregma, and DV: 4.10 mm from skull surface, 25°). All fibers and cannulae were secured in place with dental acrylic adhered to skull screws. Mice were group-housed and allowed to recover for 1 week before experimentation.

Optogenetic stimulation and 3D motion tracking

For 3D motion capture experiments, mice were connected to a 473-nm diode-pumped solid-state laser (Shanghai Laser) for optogenetic excitation (ChR2) via fiber-optic cables (105/22A, Precision Fiber) in a square open-field arena (L, 22 inches; W, 22 inches; and H, 1 inch) elevated 3 feet. The output from each sheathed optic fiber tip was measured (PM120VA, Thorlabs) before each experimental session to obtain a power between 8 and 10 mW (i.e., ~6-mW power delivered to the stimulation site with a transmittance of ~85%). A MATLAB program interfaced to a National Instruments box triggered a 5-ms^2 pulse at varying frequencies (5 to 50 Hz). Movements at a millimeter spatial resolution were captured in a Cartesian plane with eight Raptor-H digital infrared cameras (100-Hz sampling rate; Motion Analysis, CA). The cameras were placed equidistantly around the arena where two infrared spherical markers (diameter, 6.35 mm) that were located on both the fiber sleeve and tail of the mouse could be recorded. Cameras were calibrated before each experimental session. The output of the laser was channeled through an optic patch cable connected to a commutator above the open-field arena. A rotating optical commutator (Doric) divided the beam (50:50), permitting bilateral stimulation. Stimulation was triggered randomly during a 12- to 15-s interval after cessation of the previous stimulation trial using a custom MATLAB script to prevent mice from predicting the stimulation onset. Stimulation parameters were consistent within a session, but the order of stimulation (i.e., frequency and duration) was semi-randomized between mice. Unilateral and bilateral stimulation data were taken from the same animals. For unilateral experiments, separate stimulation data sessions were acquired from each hemisphere of the same animal on separate days. For pathway-specific bilateral optogenetic experiments (Fig. 4), animals were placed in an open-field arena and filmed with a camera positioned 0.7 m from the floor of the arena. Bilateral stimulation was enabled as previously described. Data were recorded on a Dell computer (16 GB RAM, Intel i7, 1 TB SSD) via a 2.0 USB adaptor at 50 f/s.

6-OHDA lesion

To generate bilateral PD mice, we injected 6-OHDA 4 weeks after viral injection and cannula implantation. Before each 6-OHDA injection, a 10-min baseline video was taken for naïve data. All mice were anesthetized with 2.5% isoflurane, and a 33-gauge injector was inserted through the cannula that extended 500 μm beyond the cannula tip. Either 6-OHDA (2.0 mg, 1300 nl per hemisphere) or vehicle (0.9% saline) was bilaterally injected using a custom microinjector and microinfusion pump (PHD 2000, Harvard Apparatus) at a rate of 100 nl/min for 2 min. The injector was withdrawn after 10 min to allow sufficient uptake of the drug. After several days (3 to 5), mice were then placed at the center of a rectangular open-field arena (L, 17.5 inches; W, 9.5 inches; and H, 6.25 inches). An open-source software program (Bonsai) using a custom script tracked movements for 10 min (*42*) The 2D coordinates based on the center of mass of each mouse were collected at 50 f/s. A baseline video (50 f/s) was first taken; then, an ABA stimulation design was used to optogenetically excite Pf-STN neurons in bilateral PD mice across various frequencies (5, 10, 25, 50, and 100 Hz). To achieve short latency control of the laser, we used two Arduinos. The first Arduino served as a data acquisition device to receive digital output signals from the computer. The second Arduino modulated frequency output from the laser using transitor-transitor logic (TTL) pulses. Stimulation conditions and equipment were the same as previously described for 3D tracking experiments. One-minute stimulation and nonstimulation epochs were interleaved in bilateral PD experiments to comprise a total duration of 30 min for each epoch during a session. Mice were allowed to rest 3 hours between stimulation sessions to prevent any movement rescue effect contamination from the previous session.

3D motion tracking analysis

A custom MATLAB script preprocessed data smoothed at 6 Hz from cortex 3D movement tracking acquisition software (Motion Analysis)

to output movement kinematic information in NeuroExplorer with respect to stimulation time stamps. Perievent histograms and rasters were generated in NeuroExplorer and analyzed in GraphPad Prism. Angular velocity kinematic data were binned at 25 ms, and the mean and SEM for each bin across experimental animals were computed to produce movement traces. Kinematic data for head and tail marker distance, head in the *z* plane, and forward velocity were standardized by a *z* score transformation. Angular velocity was not standardized because of similar velocity profiles across animals. All kinematic statistical analyses were performed on the 1 s of data preceding stimulation (Pre) compared to the 1 s of stimulation data (Stim).

Whole-cell patch clamp recording

Vglut2-ires-Cre mice were used ($n = 3$). The virus was injected into the Pf, and the animal was sacrificed 4 weeks after the injection. The brain was quickly removed and left in ice-cold solution bubbled with 95% O_2–5% CO_2 containing the following: 194 mM sucrose, 30 mM NaCl, 2.5 mM KCl, 1 mM $MgCl_2$, 26 mM $NaHCO_3$, 1.2 mM NaH_2PO_4, and 10 mM D-glucose. After 5 min, 250-μm coronal slices were cut and then placed in 35.5°C oxygenated artificial cerebrospinal fluid (aCSF) solution containing the following: 124 mM NaCl, 2.5 mM KCl, 2 mM $CaCl_2$, 1 mM $MgCl_2$, 26 mM $NaHCO_3$, 1.2 mM NaH_2PO_4, and 10 mM D-glucose. After 30 min, the slices were left in aCSF at ~22° to 23°C for at least 30 min before recording. Following recovery, all recordings were performed under continuous perfusion of aCSF at 29° to 30°C. The internal solution contained 150 mM potassium gluconate, 2 mM $MgCl_2$, 1.1 mM EGTA, 10 mM Hepes, 3 mM sodium adenosine triphosphate, and 0.2 mM sodium guanosine triphosphate. To measure the excitability of Pf neurons, each neuron was stimulated with blue light pulses (1-ms pulse width, 0.2 to 2.0 mW, 470 nm) generated at 5, 10, 25, 50, and 100 Hz for a total of 1 s by a light-emitting diode (LED) driver (Thorlabs, LEDD1B) and collimated LED (Thorlabs, M470L3) connected to a pulse generator (AMPI, Master-8). All recordings were performed with a MultiClamp 700B amplifier (Molecular Devices). Signals were filtered at 10 kHz and digitized at 20 kHz with a Digidata 1440A digitizer (Molecular Devices). The frequency of evoked action potentials was measured using peak detection software in pCLAMP10 (Molecular Devices).

Continuous behavioral classification

An unsupervised classification method was used to systematically and continuously measure behavior in pharmacological inactivation and optogenetic rescue experiments. Animals were placed in an open-field arena and filmed with a camera positioned 0.7 m from the floor of the arena. Data were recorded on a Dell computer at 50 f/s. A region of interest was outlined, and all further preprocessing was performed on the cropped image in Python using scientific tools and open source packages. Specifically, a binary threshold was applied to each frame of the video, and a 100 × 100 pixel frame was cropped around the animal. Each frame was then aligned [(*43*); https://github.com/gordonberman/MotionMapper] to eliminate allocentric components of behavior. Following the extraction and alignment of the mouse's image, a wavelet decomposition was applied to increase the dimensionality of the image for better classification of postural dynamics. Next, a principal components analysis was performed to reduce the dimensionality to the top 10 principal components. The data were then fed into an AR-HMM (*22*). The AR-HMM model takes into account the image of the mouse, the duration of the specific behavioral "syllable," and the transition probabilities to other syllables. Specifically, using Gibbs sampling with an AR-HMM will segment all of the data into distinct behavioral states and then switch to update these segments and the transitions between them (*43*). Each model goes through 1000 iterations of Gibbs sampling. All data (i.e., all groups) were cotrained to compare behavioral states across conditions. The output of the AR-HMM model allows behavioral classification into modules that occur systematically. Each video frame was assigned a behavioral label, which was used to calculate the probabilities of using each behavioral state, as well as the probabilities of transitioning between states. Following the model output, additional statistical analyses were conducted. For each mouse, bootstrapped samples were computed to assess significance in module usage, as well as transition probabilities. Group comparisons were achieved with the Hotelling's *t*-squared statistic. To assess individual differences between behavioral states, we estimated the variance of the data through bootstrapping. Using the bootstrapped estimates of variance, we performed a Wald test. We corrected for multiple comparisons using the Holm-Bonferroni method. Visualization of the data was also conducted in Python to create videos (OpenCV), graphs (NetworkX), and plots (Matplotlib).

Behavioral state and transition probability analyses

Behavioral states were classified using an AR-HMM. Videos of the states were created, and specific behaviors were characterized for the top 10 most commonly observed behaviors. Here, the probabilities of displaying each behavior are sorted by degree of mobility. The probability of each behavior is displayed separately for each group. For the transition probability analysis, the probability of using certain behaviors is displayed in the size of the nodes. The probability of transitioning between behaviors is represented by the thickness of the lines. Positions of the states are kept constant across all three panels. Initial positions are seeded using a spring algorithm, where the probability of transferring between behaviors determines the spacing of the nodes. Nodes naturally repel each other, and each connection acts like a spring pulling together nodes with strength proportional to transition probability. The behavioral usage and transition probabilities were subtracted from each other so that the remaining images represent the differences in probabilities between groups.

Transsynaptic tracing

To visualize Pf-defined cells in the STN, we used a transsynaptic tracing strategy (*24*). This technique allows for the visualization of projections from the postsynaptic neurons. In other words, a virus containing Cre recombinase can travel across the synapse and infect the postsynaptic neuron. The postsynaptic neuron can then be infected with a Cre-dependent anterograde virus to visualize the efferent projections of only those neurons receiving connections from the upstream target nuclei. To achieve this, we injected an AAV into the Pf that displays anterograde transsynaptic spread properties (AAV1.hSyn.tdTomato.Cre). This transsynaptic spread induces Cre-dependent transgene expression in the STN after injecting AAV5-DIO-eYFP. Tissue was harvested and sectioned according to the histological protocol in the next section.

Colocalization analysis with retrograde tracing

We used Fiji (https://imagej.net/Fiji/Download) to quantify the number of cells expressing both AAV-DIO-Retro2-GFP (DMS projections) and AAV-DIO-Retro2-TdTomato (STN projections) from a single coronal brain slice using 8-bit confocal images. First, we set

the threshold to identify the neuronal cell bodies; then, we used the "fill holes" function to remove possible empty space within the selected cells. After converting the image to mask, we used the "watershed" function to split cells that were too close to each other. Once these image processing steps were completed, we ran the "Analyze Particle" plug-in in Fiji to count the cells in each image. The masks obtained from the Analyze Particle function were then used to calculate the number of colocalizing cells using the "Colocalization Threshold" plug-in in Fiji.

Histology and immunohistochemistry

Mice were deeply anesthetized and perfused with 0.1 M phosphate-buffered saline (PBS) containing heparin, followed by 4% paraformaldehyde after completion of experimentation. For mice with fiber and cannula implants, heads were stored in 4% paraformaldehyde with 30% sucrose for 24 to 72 hours at 4°C to aid histological verification of placement. Brains were fixed in 30% sucrose thereafter. After sinking, brains were sliced coronally at 60 μm using a Leica CM1850 cryostat. For optogenetic experiments, the first one-in-two series of sections was processed for the presence of cytochrome oxidase to visualize cytoarchitecture. Briefly, sections were rinsed in 0.1 M phosphate buffer (PB) before incubating in a diaminobenzidine (DAB) (*44*), cytochrome C, and sucrose solution for ~2 hours at room temperature. The second series of sections were processed for Vglut2 colocalization and to enhance eYFP labeling. First, sections were rinsed in 0.1 M PBS for 20 min before being placed in a PBS-based blocking solution containing 5% goat serum and 0.25% Triton X-100 at room temperature for 1 hour. Sections were then incubated with primary antibodies [polyclonal chicken anti–green fluorescent protein (GFP), 1:500 dilution; Abcam, catalog no. ab13970; polyclonal rabbit anti-VGLUT2, 1:500 dilution; Abcam, catalog no. ab217943] in blocking solution overnight at 4°C. Sections were then rinsed in PBS for 20 min before being placed in a secondary antibody used to visualize ChR2 as marked by GFP colocalization (goat anti-chicken Alexa Fluor 488, 1:1000 dilution; Thermo Fisher Scientific, catalog no. A-11039) and Vglut2 (goat anti-rabbit Alexa Fluor 594, 1:1000 dilution; Abcam, catalog no. ab150080) for 1 hour at room temperature. We verified Vglut2 expression in virally infected neurons of *Vglut2-ires-Cre* mice against Allen Brain's in situ hybridization data online reference (gene symbol Slc17a6, experiment 73818754). Fiber placement and injection site visualization were further aided by DAPI staining in the mounting medium (Fluoromount-G) or with the neuronal marker NeuN (monoclonal rabbit anti-NeuN, 1:1000 dilution; Abcam, catalog no. ab177487). Mice were excluded from analysis if their fiber placement was not located in the target site (fig. S8). For anatomical experiments, the endogenous signal caused by CAV2-Cre injection into *Ai14* mice was not enhanced. Primary antibodies for choline acetyltransferase (monoclonal rabbit anti–choline acetyltransferase,1:1000 dilution; Abcam, catalog no. ab178850) and noradrenaline (polyclonal rabbit anti-noradrenaline, 1:500 dilution; Abcam, catalog no. ab8887) were used to identify neuronal subtype as marked by colocalization with tdTomato in the brainstem (goat anti-rabbit Alexa Fluor 488, 1:1000 dilution; Abcam, catalog no. ab150077) using the immunohistochemistry protocol previously described for eYFP enhancement. Cytochrome oxidase sections were dehydrated in 200-proof ethanol, defatted in xylene, and coverslipped with Cytoseal. Sections for fluorescent microscopy were mounted and immediately coverslipped with Fluoromount aqueous mounting medium (Sigma-Aldrich, catalog no. F4680). Bright-field images were acquired and stitched using an Axio Imager M1 upright microscope (Zeiss), and fluorescent images were acquired and stitched using a Z10 inverted microscope (Zeiss). Confirmation of optical fiber placement was performed by comparing images with a mouse brain atlas (*45*).

Tyrosine hydroxylase processing and quantification

A tyrosine hydroxylase reaction was performed to visualize pallidal and striatal dopaminergic cell death in 6-OHDA–injected mice. Briefly, sections were first agitated in a 3% H_2O_2 solution for 10 min at room temperature to block endogenous peroxidases. Sections were then transferred to a PBS-based blocking solution containing 5% goat serum and 0.25% Triton X-100 at room temperature for 1 hour. After incubating overnight in blocking solution containing a primary antibody (polyclonal rabbit anti–tyrosine hydroxylase, 1:1000 dilution; Millipore, catalog no. 657012), sections were incubated for 1 hour at room temperature in a biotinylated solution (biotinylated goat anti-rabbit immunoglobulin G, 1:200 dilution; Vector Laboratories, catalog no. BA-1000) before incubating in an avidin-biotin horseradish peroxidase solution for 2 hours at room temperature (Vector Novocastra Laboratories). After rinsing sections in PBS, tyrosine hydroxylase neurons were visualized with 0.05% DAB and 0.005% H_2O_2 in double distilled H_2O (pH 7.2) for 5 to 10 min. The DAB reaction was stopped with subsequent PBS washes and stored at 4°C. Tyrosine hydroxylase–reacted sections were dehydrated in 200-proof ethanol, defatted in xylene, and coverslipped with Cytoseal. The intensity of tyrosine hydroxylase staining in saline-injected ($n = 3$) and bilateral PD experimental groups ($n = 10$) was quantified as previously described (*21*). Bilateral PD animals were included in analyses if tyrosine hydroxylase intensity values were <80% compared to controls. Two bilateral PD animals were excluded from the study because they did not meet this criterion.

Quantification and statistical analysis

The values and error bars reported in the text are the mean ± SEM, respectively. Behavioral data were analyzed with MATLAB 2016b (MathWorks). Statistical tests were performed in Prism 8 (GraphPad). Two-tailed parametric tests were used. An a priori alpha level of 0.05 was used to determine significance.

SUPPLEMENTARY MATERIALS

Supplementary material for this article is available at http://advances.sciencemag.org/cgi/content/full/7/6/eabe9192/DC1

View/request a protocol for this paper from *Bio-protocol*.

REFERENCES AND NOTES

1. C. R. Gerfen, C. J. Wilson, The basal ganglia, in *Handbook of Chemical Neuroanatomy*, L. W. Swanson, A. Bjorklund, T. Hokfelt, Eds. (Elsevier, 1996), vol. 12, pp. 371–468.
2. B. J. Hunnicutt, B. C. Jongbloets, W. T. Birdsong, K. J. Gertz, H. Zhong, T. Mao, A comprehensive excitatory input map of the striatum reveals novel functional organization. *eLife* **5**, e19103 (2016).
3. Y. Smith, A. Galvan, T. J. Ellender, N. Doig, R. M. Villalba, I. H. Ocampo, T. Wichman, J. P. Bolam, The thalamostriatal system in normal and diseased states. *Front. Syst. Neurosci.* **8**, 5 (2014).
4. N. Matsumoto, T. Minamimoto, A. M. Graybiel, M. Kimura, Neurons in the thalamic CM-Pf complex supply striatal neurons with information about behaviorally significant sensory events. *J. Neurophysiol.* **85**, 960–976 (2001).
5. H. D. Brown, P. M. Baker, M. E. Ragozzino, The parafascicular thalamic nucleus concomitantly influences behavioral flexibility and dorsomedial striatal acetylcholine output in rats. *J. Neurosci.* **30**, 14390–14398 (2010).
6. A. Tanimura, Y. Du, J. Kondapalli, D. L. Wokosin, D. J. Surmeier, Cholinergic interneurons amplify thalamostriatal excitation of striatal indirect pathway neurons in Parkinson's disease models. *Neuron* **101**, 444–458.e6 (2019).

7. D. Anderson, G. Beecher, F. Ba, Deep brain stimulation in Parkinson's disease: New and emerging targets for refractory motor and nonmotor symptoms. *Parkinsons Dis.* **2017**, 5124328 (2017).
8. L. Kerkerian-Le Goff, L. Jouve, C. Melon, P. Salin, Rationale for targeting the thalamic centre-median parafascicular complex in the surgical treatment of Parkinson's disease. *Parkinsonism Relat. Disord.* **15** (Suppl 3), S167–S170 (2009).
9. P. Mazzone, F. Stocchi, S. Galati, A. Insola, M. G. Altibrandi, N. Modugno, D. Tropepi, L. Brusa, A. Stefani, Bilateral implantation of centromedian-parafascicularis complex and GPi: A new combination of unconventional targets for deep brain stimulation in severe Parkinson disease. *Neuromodulation* **9**, 221–228 (2006).
10. A. Peppe, A. Gasbarra, A. Stefani, C. Chiavalon, M. Pierantozzi, E. Fermi, P. Stanzione, C. Caltagirone, P. Mazzone, Deep brain stimulation of CM/PF of thalamus could be the new elective target for tremor in advanced Parkinson's disease? *Parkinsonism Relat. Disord.* **14**, 501–504 (2008).
11. A. Stefani, A. Peppe, M. Pierantozzi, S. Galati, V. Moschella, P. Stanzione, P. Mazzone, Multi-target strategy for Parkinsonian patients: The role of deep brain stimulation in the centromedian-parafascicularis complex. *Brain Res. Bull.* **78**, 113–118 (2009).
12. P. R. L. Parker, A. L. Lalive, A. C. Kreitzer, Pathway-specific remodeling of thalamostriatal synapses in parkinsonian mice. *Neuron* **89**, 734–740 (2016).
13. T. Kita, N. Shigematsu, H. Kita, Intralaminar and tectal projections to the subthalamus in the rat. *Eur. J. Neurosci.* **44**, 2899–2908 (2016).
14. G. J. Royce, R. J. Mourey, Efferent connections of the centromedian and parafascicular thalamic nuclei: An autoradiographic investigation in the cat. *J. Comp. Neurol.* **235**, 277–300 (1985).
15. J. Feger, M. Bevan, A. R. Crossman, The projections from the parafascicular thalamic nucleus to the subthalamic nucleus and the striatum arise from separate neuronal populations: A comparison with the corticostriatal and corticosubthalamic efferents in a retrograde fluorescent double-labelling study. *Neuroscience* **60**, 125–132 (1994).
16. G. Mandelbaum, J. Taranda, T. M. Haynes, D. R. Hochbaum, K. W. Huang, M. Hyun, K. U. Venkataraju, C. Straub, W. Wang, K. Robertson, Distinct cortical-thalamic-striatal circuits through the parafascicular nucleus. *Neuron* **102**, 636–652.e7 (2019).
17. R. T. Fremeau Jr., M. D. Troyer, I. Pahner, G. O. Nygaard, C. H. Tran, R. J. Reimer, E. E. Bellocchio, D. Fortin, J. Storm-Mathisen, R. H. Edwards, The expression of vesicular glutamate transporters defines two classes of excitatory synapse. *Neuron* **31**, 247–260 (2001).
18. W. Lei, Y. Deng, B. Liu, S. Mu, N. M. Guley, T. Wong, A. Reiner, Confocal laser scanning microscopy and ultrastructural study of VGLUT2 thalamic input to striatal projection neurons in rats. *J. Comp. Neurol.* **521**, 1354–1377 (2013).
19. D. G. Tervo, B. Y. Hwang, S. Viswanathan, T. Gaj, M. Lavzin, K. D. Ritola, S. Lindo, S. Michael, E. Kuleshova, D. Ojala, C. C. Huang, C. R. Gerfen, J. Schiller, J. T. Dudman, A. W. Hantman, L. L. Looger, D. V. Schaffer, A. Y. Karpova, A designer AAV variant permits efficient retrograde access to projection neurons. *Neuron* **92**, 372–382 (2016).
20. S. L. Thiele, R. Warre, J. E. Nash, Development of a unilaterally-lesioned 6-OHDA mouse model of Parkinson's disease. *J. Vis. Exp.*, 3234 (2012).
21. K. J. Mastro, K. T. Zitelli, A. M. Willard, K. H. Leblanc, A. V. Kravitz, A. H. Gittis, Cell-specific pallidal intervention induces long-lasting motor recovery in dopamine-depleted mice. *Nat. Neurosci.* **20**, 815–823 (2017).
22. A. B. Wiltschko, M. J. Johnson, G. Iurilli, R. E. Peterson, J. M. Katon, S. L. Pashkovski, V. E. Abraira, R. P. Adams, S. R. Datta, Mapping sub-second structure in mouse behavior. *Neuron* **88**, 1121–1135 (2015).
23. J. E. Markowitz, W. F. Gillis, C. C. Beron, S. Q. Neufeld, K. Robertson, N. D. Bhagat, R. E. Peterson, E. Peterson, M. Hyun, S. W. Linderman, B. L. Sabatini, S. R. Datta, The striatum organizes 3D behavior via moment-to-moment action selection. *Cell* **174**, 44–58.e17 (2018).
24. B. Zingg, X. L. Chou, Z. G. Zhang, L. Mesik, F. Liang, H. W. Tao, L. I. Zhang, AAV-mediated anterograde transsynaptic tagging: Mapping corticocollicular input-defined neural pathways for defense behaviors. *Neuron* **93**, 33–47 (2017).
25. M. L. Porceddu, B. Piacente, M. Morelli, G. Di Chiara, Opposite turning effects of dainic and ibotenic acid injected in the rat substantia nigra. *Neurosci. Lett.* **15**, 271–276 (1979).
26. J. W. Barter, S. Castro, T. Sukharnikova, M. A. Rossi, H. H. Yin, The role of the substantia nigra in posture control. *Eur. J. Neurosci.* **39**, 1465–1473 (2014).
27. C. R. Gerfen, D. J. Surmeier, Modulation of striatal projection systems by dopamine. *Annu. Rev. Neurosci.* **34**, 441–466 (2011).
28. F. Tecuapetla, S. Matias, G. P. Dugue, Z. F. Mainen, R. M. Costa, Balanced activity in basal ganglia projection pathways is critical for contraversive movements. *Nat. Commun.* **5**, 4315 (2014).
29. R. A. Bartholomew, H. Li, E. J. Gaidis, M. Stackmann, C. T. Shoemaker, M. A. Rossi, H. H. Yin, Striatonigral control of movement velocity in mice. *Eur. J. Neurosci.* **43**, 1097–1110 (2016).
30. A. V. Kravitz, B. S. Freeze, P. R. Parker, K. Kay, M. T. Thwin, K. Deisseroth, A. C. Kreitzer, Regulation of parkinsonian motor behaviours by optogenetic control of basal ganglia circuitry. *Nature* **466**, 622–626 (2010).
31. A. Nambu, H. Tokuno, M. Takada, Functional significance of the cortico-subthalamo-pallidal 'hyperdirect' pathway. *Neurosci. Res.* **43**, 111–117 (2002).
32. J. D. Schaafsma, Y. Balash, T. Gurevich, A. L. Bartels, J. M. Hausdorff, N. Giladi, Characterization of freezing of gait subtypes and the response of each to levodopa in Parkinson's disease. *Eur. J. Neurol.* **10**, 391–398 (2003).
33. J. D. Schaafsma, N. Giladi, Y. Balash, A. L. Bartels, T. Gurevich, J. M. Hausdorff, Gait dynamics in Parkinson's disease: Relationship to parkinsonian features, falls and response to levodopa. *J. Neurol. Sci.* **212**, 47–53 (2003).
34. J. Nonnekes, M. H. Timmer, N. M. de Vries, O. Rascol, R. C. Helmich, B. R. Bloem, Unmasking levodopa resistance in Parkinson's disease. *Mov. Disord.* **31**, 1602–1609 (2016).
35. M. S. Remple, C. H. Bradenham, C. C. Kao, P. D. Charles, J. S. Neimat, P. E. Konrad, Subthalamic nucleus neuronal firing rate increases with Parkinson's disease progression. *Mov. Disord.* **26**, 1657–1662 (2011).
36. S. Miocinovic, S. Somayajula, S. Chitnis, J. L. Vitek, History, applications, and mechanisms of deep brain stimulation. *JAMA Neurol.* **70**, 163–171 (2013).
37. V. Gradinaru, M. Mogri, K. R. Thompson, J. M. Henderson, K. Deisseroth, Optical deconstruction of parkinsonian neural circuitry. *Science* **324**, 354–359 (2009).
38. K. J. Mastro, R. S. Bouchard, H. A. Holt, A. H. Gittis, Transgenic mouse lines subdivide external segment of the globus pallidus (GPe) neurons and reveal distinct GPe output pathways. *J. Neurosci.* **34**, 2087–2099 (2014).
39. J. L. Lanciego, I. P. Lopez, A. J. Rico, M. S. Aymerich, M. Perez-Manso, L. Conte, C. Combarro, E. Roda, C. Molina, N. Gonzalo, M. Castle, T. Tunon, E. Erro, P. Barroso-Chinea, The search for a role of the caudal intralaminar nuclei in the pathophysiology of Parkinson's disease. *Brain Res. Bull.* **78**, 55–59 (2009).
40. C. Yu, I. R. Cassar, J. Sambangi, W. M. Grill, Frequency-specific optogenetic deep brain stimulation of subthalamic nucleus improves parkinsonian motor behaviors. *J. Neurosci.* **40**, 4323–4334 (2020).
41. W. Thevathasan, B. Debu, T. Aziz, B. R. Bloem, C. Blahak, C. Butson, V. Czernecki, T. Foltynie, V. Fraix, D. Grabli, C. Joint, A. M. Lozano, M. S. Okun, J. Ostrem, N. Pavese, C. Schrader, C. H. Tai, J. K. Krauss, E. Moro; Movement Disorders Society PPN DBS Working Groupin collaboration with the World Society for Stereotactic and Functional Neurosurgery, Pedunculopontine nucleus deep brain stimulation in Parkinson's disease: A clinical review. *Mov. Disord.* **33**, 10–20 (2018).
42. G. Lopes, N. Bonacchi, J. Frazao, J. P. Neto, B. V. Atallah, S. Soares, L. Moreira, S. Matias, P. M. Itskov, P. A. Correia, R. E. Medina, L. Calcaterra, E. Dreosti, J. J. Paton, A. R. Kampff, Bonsai: An event-based framework for processing and controlling data streams. *Front. Neuroinform.* **9**, 7 (2015).
43. G. J. Berman, D. M. Choi, W. Bialek, J. W. Shaevitz, Mapping the stereotyped behaviour of freely moving fruit flies. *J. R. Soc. Interface* **11**, 20140672 (2014).
44. J. M. Henderson, S. B. Schleimer, H. Allbutt, V. Dabholkar, D. Abela, J. Jovic, M. Quinlivan, Behavioural effects of parafascicular thalamic lesions in an animal model of parkinsonism. *Behav. Brain Res.* **162**, 222–232 (2005).
45. G. P. K. B. J. Franklin, in *The Mouse Brain in Stereotaxic Coordinates* (Academic Press, ed. 4, 2012), pp. 360.

Acknowledgments: We thank F, Allen, E. Gaidis, and A. Friedman for technical assistance and M. Tadross and N. Calakos for helpful comments on the manuscript. **Funding:** This work was supported by grants NS094754 and MH112883 awarded to H.H.Y. **Author contributions:** Conceptualization: G.D.R.W. and H.H.Y conceptualized and designed experiments. G.D.R.W., R.N.H., and E.A.P wrote analysis code. G.D.R.W. F.P.U.S., I.P.F., and R.N.H. performed confocal microscopy. G.D.R.W., I.P.F., and R.N.H. performed surgeries. G.D.R.W. and R.N.H. performed behavioral experiments an in vivo electrophysiology, N.H. performed in vitro electrophysiology. Data analysis was performed by G.D.R.W., R.N.H., N.K., and E.A.P. Cell quantification was performed by F.P.U.S. G.D.R.W., R.N.H., and H.H.Y wrote and edited the manuscript. **Competing interests:** The authors declare that they have no competing interests. **Data and materials availability:** All data needed to evaluate the conclusions in the paper are present in the paper and/or the Supplementary Materials. Additional data related to this paper may be requested from the authors.

Submitted 22 September 2020
Accepted 21 December 2020
Published 5 February 2021
10.1126/sciadv.abe9192

Citation: G. D. R. Watson, R. N. Hughes, E. A. Petter, I. P. Fallon, N. Kim, F. P. U. Severino, H. H. Yin, Thalamic projections to the subthalamic nucleus contribute to movement initiation and rescue of parkinsonian symptoms. *Sci. Adv.* **7**, eabe9192 (2021).